Imaging protein interactions with bioluminescence resonance energy transfer (BRET) in plant and mammalian cells and tissues

Xiaodong Xu*, Mohammed Soutto*, Qiguang Xie*, Stein Servick*, Chitra Subramanian†, Albrecht G. von Arnim†, and Carl Hirschie Johnson*‡

*Department of Biological Sciences, Box 1634-B, Vanderbilt University, Nashville, TN 37235; and †Department of Biochemistry and Cellular and Molecular Biology, University of Tennessee, Knoxville, TN 37996

Edited by J. Woodland Hastings, Harvard University, Cambridge, MA, and approved April 16, 2007 (received for review March 3, 2007)

FRET is a well established method for cellular and subcellular imaging of protein interactions. However, FRET obligatorily necessitates fluorescence excitation with its concomitant problems of photobleaching, autofluorescence, phototoxicity, and undesirable stimulation of photobiological processes. A sister technique, bioluminescence resonance energy transfer (BRET), avoids these problems because it uses enzyme-catalyzed luminescence; however, BRET signals usually have been too dim to image effectively in the past. Using a new generation electron bombardment-charge-coupled device camera coupled to an image splitter, we demonstrate that BRET can be used to image protein interactions in plant and animal cells and in tissues; even subcellular imaging is possible. We have applied this technology to image two different protein interactions: (*i*) dimerization of the developmental regulator, COP1, in plant seedlings; and (*ii*) CCAAT/enhancer binding protein α (C/EBPα) in the mammalian nucleus. This advance heralds a host of applications for imaging without fluorescent excitation and its consequent limitations.

C/EBP | COP1 | FRET | luminescence | fluorescence

Interactions among proteins are key to the performance of their cellular activity. Identifying the partners with which a protein associates has been a major approach, in addition to genetics, toward discovering the key components of a biological pathway. Moreover, quantifying and localizing these protein interactions are crucial to the ultimate understanding of how proteins accomplish their *raison d'etre*. Many different methods are available for measuring protein interactions (1), but one of the most useful is based on Förster resonance energy transfer (2). In particular, FRET is a well established resonance energy technique for monitoring protein interactions (3). When two fluorophores (the "donor" and the "acceptor") with overlapping emission/absorption spectra are within ≈50 Å of one another and other conditions are met, the donor fluorophore is able to transfer its excited-state energy to the acceptor fluorophore. FRET can act as a "molecular yardstick" when two fluorophores of overlapping emission/absorption spectra are within a radius of ≈50 Å and other conditions are met. Therefore, if appropriate fluorophores are linked to proteins that interact with each other, the proximity of those proteins can be detected by FRET in living cells in which the fusion proteins are produced endogenously (3). Thus, the presence or absence of FRET acts as a molecular yardstick.

However, because FRET demands that the donor fluorophore be excited by light, the practical usefulness of FRET can be limited by the concomitant consequences of that irradiation: photobleaching, autofluorescence, and direct excitation of the acceptor fluorophore. Furthermore, some tissues can be damaged by the excitation light or might be directly photoresponsive (e.g., retina and most plant tissues) so that a photobiologically regulated interaction can be disturbed by FRET. For these reasons, we developed a complementary technique, bioluminescence resonance energy transfer (BRET) (4), that takes advantage of the natural phenomenon in which GFP participates (5). In BRET, the donor fluorophore of the FRET technique is replaced by a luciferase. In the presence of a substrate, bioluminescence emanating from the luciferase can excite the acceptor fluorophore if the luciferase and fluorophore are within a radius of ≈50 Å. BRET thereby avoids the problems of direct excitation while retaining the advantages of FRET. BRET also has the potential to outshine FRET for deep penetration of animal tissues (6) and for high-throughput screening because an internal light source is not required in the screening instrument and because BRET does not photobleach the energy donor (7).

On the other hand, because the light emission from BRET generally is dim, it has been thought to be less suitable for imaging than is FRET (8, 9). In particular, BRET has been thought to be "not currently suitable for single-cell analyses and thus information on cellular distribution and spatial resolution cannot be provided" with BRET (7). Until now, that is. We have coupled a very sensitive charge-coupled device (CCD) camera with a Dual-View image splitter to display BRET localizations in highly autofluorescent plant tissues and cells. Here, we present the tissue localization for dimerization of the plant regulator of light signaling, constitutive photomorphogenesis 1 (COP1) protein. Furthermore, we are able to image the subcellular distributions of interactions of the CCAAT/enhancer binding protein α (C/EBPα) in single isolated mammalian cells. This advance augurs imaging applications that are not limited by problems associated with fluorescent excitation.

Results

Imaging of BRET Interactions in Whole Tobacco Seedlings. Although low-resolution BRET imaging has been reported for whole-animal imaging (6), Fig. 1 demonstrates that BRET imaging at a higher level of resolution can be applied to plant seedlings by using a modified electron bombardment-CCD (EB-CCD) camera and a Dual-View microimager attached directly to a ×4 microscopic objective. The microimager allows us to collect two wavelength ranges simultaneously by including a dichroic that splits the image at 505 nm and short-pass/long-pass filters that refine the spectral

Author contributions: X.X. and M.S. contributed equally to this work. X.X., M.S., and C.H.J. designed research; X.X., M.S., Q.X., and S.S. performed research; C.S. and A.G.v.A. contributed new reagents/analytic tools; X.X., M.S., Q.X., and C.H.J. analyzed data; and C.H.J. wrote the paper.

The authors declare no conflict of interest.

This article is a PNAS Direct Submission.

Abbreviations: BRET, bioluminescence resonance energy transfer; CCD, charge-coupled device; COP1, constitutive photomorphogenesis 1; EB-CCD, electron bombardment-CCD; RLUC, *Renilla* luciferase; EYFP, enhanced yellow fluorescent protein; hRLUC, "humanized" RLUC; NA, numerical aperture.

See Commentary on page 9917.

‡To whom correspondence should be addressed. E-mail: carl.h.johnson@vanderbilt.edu.

This article contains supporting information online at www.pnas.org/cgi/content/full/0701987104/DC1.

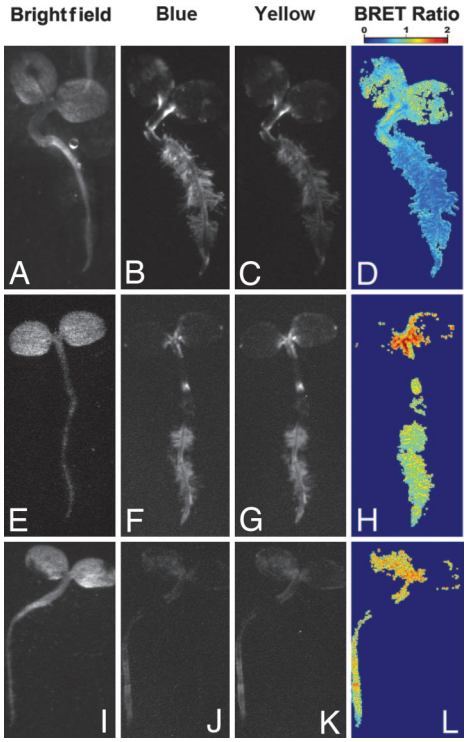

Fig. 1. BRET macroimaging of tobacco seedlings using the light-tight box apparatus (see *SI Text*). (*A–L*) Tobacco seedlings ≈7 days after germination. Shown are seedlings transformed with (*i*) P_{35S}::Rluc (*A–D*), (*ii*) P_{35S}::Rluc·EYFP (*E–H*), and (*iii*) P_{35S}::Rluc·COP1 + P_{35S}::EYFP·COP1 (*I–L*). (*A*, *E*, and *I*) Bright-field images. (*B*, *F*, and *J*) Short-pass luminescence images (blue). (*C*, *G*, and *K*) Long-pass luminescence images (yellow). (*D*, *H*, and *L*) BRET ratios (Y÷B) over the entire image (pseudocolor scale is shown above *D*). Quantification of the average BRET ratios (Y÷B ± SD) over the entire images for these samples are as follows: for RLUC, Y÷B = 0.85 ± 0.08 SD (n = 4, including *D*); for RLUC·EYFP, Y÷B = 1.31 ± 0.15 SD (n = 3, including *H*); and for RLUC·COP1/EYFP·COP1, Y÷B = 1.26 ± 0.12 SD (n = 4, including *L*). A ×4 noninfinity-corrected microscopic objective was coupled directly to the Dual-View, which was connected in turn to the EB-CCD camera. Exposure time averaged 7.5 min. Coelenterazine concentration was 10 μM at 22°C.

distinction [see supporting information (SI) *Text*]. The spectra distinguished by the Dual-View are (*i*) wavelengths shorter than 505 nm (= B for blue light) versus (*ii*) wavelengths longer than 505 nm (= Y for yellow light; see SI Fig. 5). A "BRET ratio" then is derived over the image to quantify the amount of resonance transfer from luciferase to fluorophore, and these BRET ratios will be expressed herein as "Y÷B" or "Y:B." Fig. 1 *A–D* depicts the BRET signal when *Renilla* luciferase (RLUC) is expressed alone in tobacco seedlings. RLUC luminescence is expressed strongly from root hairs as well as stems and weakly from cotyledons (Fig. 1 *B* and *C*). As expected, the luminescence image for RLUC in the blue window (Fig. 1*B*) is significantly brighter than that in the yellow window (Fig. 1*C*), resulting in a BRET ratio over the entire seedling that is mostly <1.0 (average Y:B over the entire image = 0.85 ± 0.08 SD; Fig. 1*D*). On the other hand, luminescence from the fusion protein RLUC·enhanced yellow fluorescent protein (EYFP), which exhibits BRET (4), shows a brighter luminescence in the yellow than in the blue (Fig. 1 *F* and *G*), resulting in a BRET ratio over the seedling predominantly >1.0 (Y:B = 1.31 ± 0.15 SD; Fig. 1*H*).

We previously showed in a nonimaging study that BRET could be used to measure the dimerization of COP1 protein, a repressor of light-regulated development in plants (10, 11). Because that investigation was performed in onion epidermal cells, it could not demonstrate the localization of COP1 interaction among the tissues of seedlings/plants. Here, we use BRET to visualize the tissue localization of COP1 dimerization in tobacco seedlings with two independent COP1 fusion proteins; both fusion proteins are N-terminal fusions: RLUC·COP1 and EYFP·COP1 (10). These constructs were not expressed as strongly in the tobacco seedlings as were RLUC and RLUC·EYFP, but they clearly were expressed in the rootlet and cotyledons (Fig. 1 *J–K*). The BRET ratio was high (Y:B = 1.26 ± 0.12 SD) wherever the RLUC·COP1 expression was strong enough to obtain a detectable luminescence image (Fig. 1*L*). This result indicates that dimerization occurs for the photomorphogenesis-regulating protein COP1 throughout the seedling, even in tissues such as roots that do not normally receive strong illumination and therefore would not be expected to express pathways involved in light-regulated development.

BRET Imaging in *Arabidopsis* Tissues and Cells. Fig. 1 clearly shows that macroimaging of plant tissue BRET is possible. We decided to zoom in with an inverted microscope coupled with our EB-CCD/Dual-View on specific tissues and cells of *Arabidopsis*, the most widely used plant for genetic research. Fig. 2 illustrates the application of BRET to the cotyledons of seedlings (Fig. 2 *A–I*) and to a single isolated plant cell (Fig. 2 *J–N*). Fig. 2*A* shows spectra of whole *Arabidopsis* seedlings expressing RLUC or RLUC·EYFP. Fig. 2 *B* and *C* shows the emission of RLUC-expressing seedlings in the blue and the yellow, respectively. Fig. 2*D* shows the BRET ratio over the cotyledons, which generally is <1.0 (Y:B = 0.58 ± 0.02 SD), which corresponds well with that expected from the whole-seedling spectrum shown in Fig. 2*A*. Fig. 2 *E–I* shows another cotyledon expressing the RLUC·EYFP fusion protein. By virtue of its EYFP moiety, this protein is fluorescent, and therefore the distribution of its fluorescence over the cotyledon can be visualized (Fig. 2*F*). Assay of luminescence demonstrates that the yellow emission (Fig. 2*H*) is brighter than the blue emission (Fig. 2*G*), resulting in a BRET ratio >1.0 (Y:B = 1.18 ± 0.05 SD; Fig. 2*I*), as expected from the whole-seedling BRET spectrum (Fig. 2*A*).

We then extended BRET imaging to single *Arabidopsis* cells isolated from a suspension culture line and expressing the RLUC·EYFP fusion protein (Fig. 2 *J–N*). As was the case for cotyledon tissue, single cells expressing RLUC·EYFP exhibit fluorescence (Fig. 2*K*) and luminescence that is brighter in the yellow (Fig. 2*M*) than in the blue (Fig. 2*L*), resulting in a BRET ratio >1.0 (Fig. 2*N*). RLUC·EYFP is localized in the cytoplasm (the outer ring) and the nucleus (the bulge at the 10 o'clock position of the ring) but is excluded from the large central vacuole that is characteristic of most plant cells.

Correction of BRET Signal in Differentially Absorbing Tissues. In our measurements of RLUC·EYFP emission in *Escherichia coli* (4) and mammalian cells (see below), the emission peaks in the blue versus the yellow windows have been approximately equal (i.e., Y:B ≈ 1.0). Therefore, we initially were perplexed that the yellow peak was reproducibly higher when RLUC·EYFP was expressed in plant tissue (as in Fig. 2*A*). We considered the possibility that this was because of the fact that green plant tissue contains many pigments that might differentially absorb luminescence of different wavelengths. This hypothesis is easily tested because plants can be germinated and grown in darkness, resulting in "etiolated" or essentially nonpigmented tissue. When we measured the whole-plant emission spectrum of RLUC·EYFP from etiolated tobacco seedlings, we indeed found an emission spectrum that was closer to 1:1 for Y:B (Fig. 3*A*). Data from imaging of "green" versus "etiolated" seedlings bore out this hypothesis: for RLUC-expressing seedlings, Y:B = 0.85 ± 0.08 SD for green seedlings, but Y:B = 0.54 ± 0.14 SD for etiolated seedlings; for RLUC·EYFP-expressing seedlings, Y:B = 1.31 ± 0.15 SD for green seedlings, but Y:B = 0.98 ± 0.04 for etiolated seedlings; and for RLUC·COP1/EYFP·COP1-

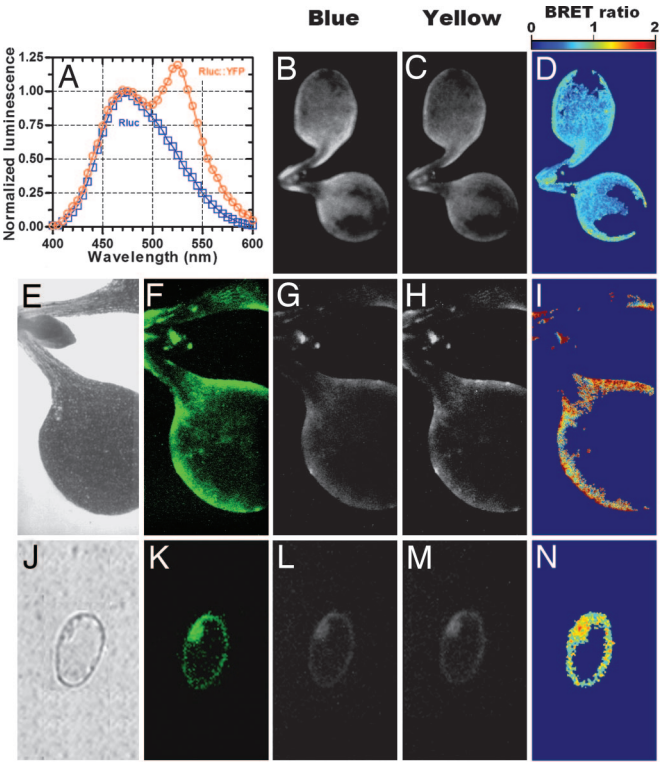

Fig. 2. BRET microimaging of *Arabidopsis* seedlings using an inverted fluorescence microscope apparatus. (*A*) Spectra of RLUC and RLUC·YFP emission from whole *Arabidopsis* seedlings. Luminescence spectra were normalized to the emission at 480 nm. Shown are seedlings transformed with (*i*) P_{35S}::Rluc (*B–D*) (no bright-field image is available for this sample, and because RLUC is not fluorescent, there is no fluorescence image), and (*ii*) P_{35S}::Rluc·EYFP (*E–I*) (optics arrangement 1 with ×2 objective, 5-min exposure time). (*J–N*) A single isolated *Arabidopsis* cell expressing RLUC·EYFP from a suspension culture [optics arrangement 2 with ×40 objective, N.A. 1.30 (oil immersion), 7.5-min exposure time]. (*E* and *J*) Bright-field images. (*F* and *K*) RLUC·EYFP fusion protein's fluorescence images. (*B*, *G*, and *L*) Short-pass luminescence (blue) images. (*C*, *H*, and *M*) Long-pass luminescence images (yellow). (*D*, *I*, and *N*) BRET ratios (Y÷B) over the entire image (pseudocolor scale shown above *D*). Quantification of the average BRET ratios (Y÷B ± SD) over the entire images for these samples are as follows: for RLUC, Y÷B = 0.58 ± 0.02 SD (n = 6, including *D*); and for RLUC·EYFP, Y÷B = 1.18 ± 0.05 SD (n = 6, including *I*). Coelenterazine concentration was 10 μM at 22°C.

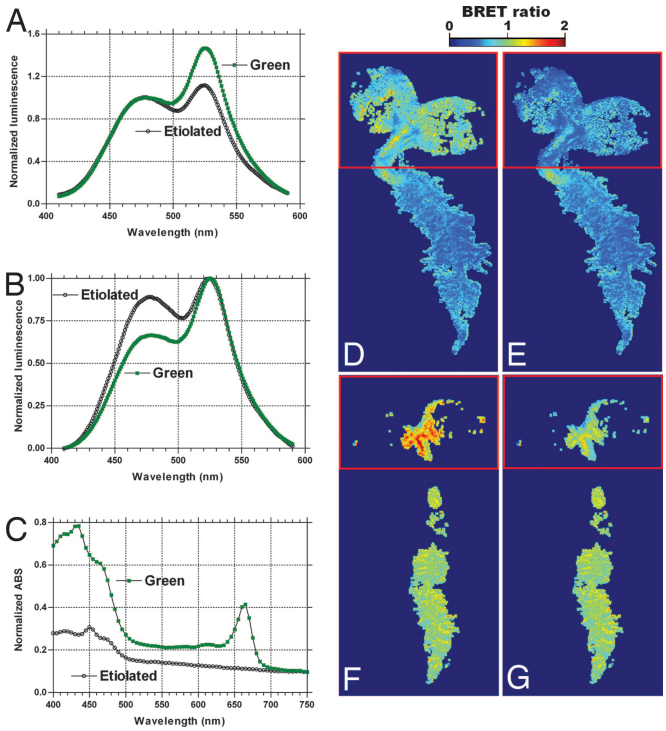

Fig. 3. Correction of BRET images from plants for differential absorption of luminescence. (*A*) RLUC·EYFP emission spectra for light-grown (green) and dark-grown (etiolated) tobacco seedlings, normalized to the emission at 480 nm. (*B*) RLUC·EYFP emission spectra for green and etiolated tobacco seedlings, normalized to the emission at 530 nm. (*C*) Absorption spectra of an ethanol extraction of pigments from green and etiolated tobacco seedlings. (*D* and *E*) *D* shows the BRET ratio image from Fig. 1*D*, shown with a red box encasing the pigmented (cotyledon) portion that is corrected in *E*. (*F* and *G*) *F* shows the BRET ratio image from Fig. 1*H*, shown with a red box encasing the cotyledon portion that is corrected in *G*. Correction factor for boxed regions of *E* and *G* was 1.27 (see *SI Text*).

expressing seedlings, Y:B = 1.26 ± 0.12 SD for green seedlings, but Y:B = 0.96 ± 0.01 SD for etiolated seedlings (BRET images for etiolated seedlings are not shown).

Green plant tissue contains pigments that absorb more strongly in the blue than in the green–yellow regions of the spectrum, as can be seen by the luminescence spectra normalized to 530 nm (Fig. 3*B*) and by absorption spectra of extracted plant tissue (Fig. 3*C*). This information can be used to normalize spectra for use in quantitative BRET assays. For example, we calculate that the absorption at 480 nm is 1.27× that at 530 nm (see *SI Text*), so we can correct our BRET images for this differential absorption, as illustrated in Fig. 3. Fig. 3*D* is the uncorrected image of an RLUC-expressing seedling (same BRET ratio image shown in Fig. 1*D*), and Fig. 3*E* has been corrected over the area of the image that is the green cotyledon tissue (upper region encased in red box; the root region of seedlings is not pigmented). Within this corrected region, the BRET ratio for RLUC emission now is 0.57, which is close to the value obtained for RLUC emission from etiolated seedlings (Y:B = 0.54 ± 0.14; see preceding paragraph). For an RLUC·EYFP-expressing seedling, Fig. 3*F* is an uncorrected image (same BRET ratio image shown in Fig. 1*H*), whereas Fig. 3*G* has been corrected over the area of the image that is the pigmented cotyledon tissue (red box). Within this corrected region, the BRET ratio for RLUC emission now is 0.97, which is more similar to the values obtained for RLUC·EYFP emission from etiolated seedlings (Y:B = 0.98 ± 0.04; see preceding paragraph), RLUC·EYFP emission from bacterial cells (4), and "humanized" RLUC (i.e., sequence optimized for human codon bias) (hRLUC)·Venus (optimized YFP) emission from mammalian cells (see Fig. 4*I*). Note that after correction, the seedlings in Fig. 3 *E* and *G* show equivalent BRET ratios over the green cotyledon (red box areas) and nonpigmented root regions.

Subcellular Imaging of BRET Interactions in Single Mammalian Cells. BRET imaging also is possible from single mammalian cells in serum-containing medium by using the coelenterazine analog ViviRen as the substrate for RLUC (see *SI Text* and SI Fig. 6 for a discussion of the relative merits of native coelenterazine versus its analogs as substrates for BRET imaging). Fig. 4 shows images from both human HEK293 and mouse GHFT1 cells transfected with various BRET constructs. A comparison of the bright-field images (Fig. 4 *A*, *F*, *K*, *P*, *U*, and *Z*) with the luminescence and fluorescence images shows that the transfection efficiency was rather low, with usually a single cell transfected within the field of view (Fig. 4 *A–D* is an exception, where two cells are transfected). Fig. 4 *A–D* shows HEK293 cells transfected with hRLUC; these cells exhibit a low BRET ratio (Y:B = 0.32 ± 0.05

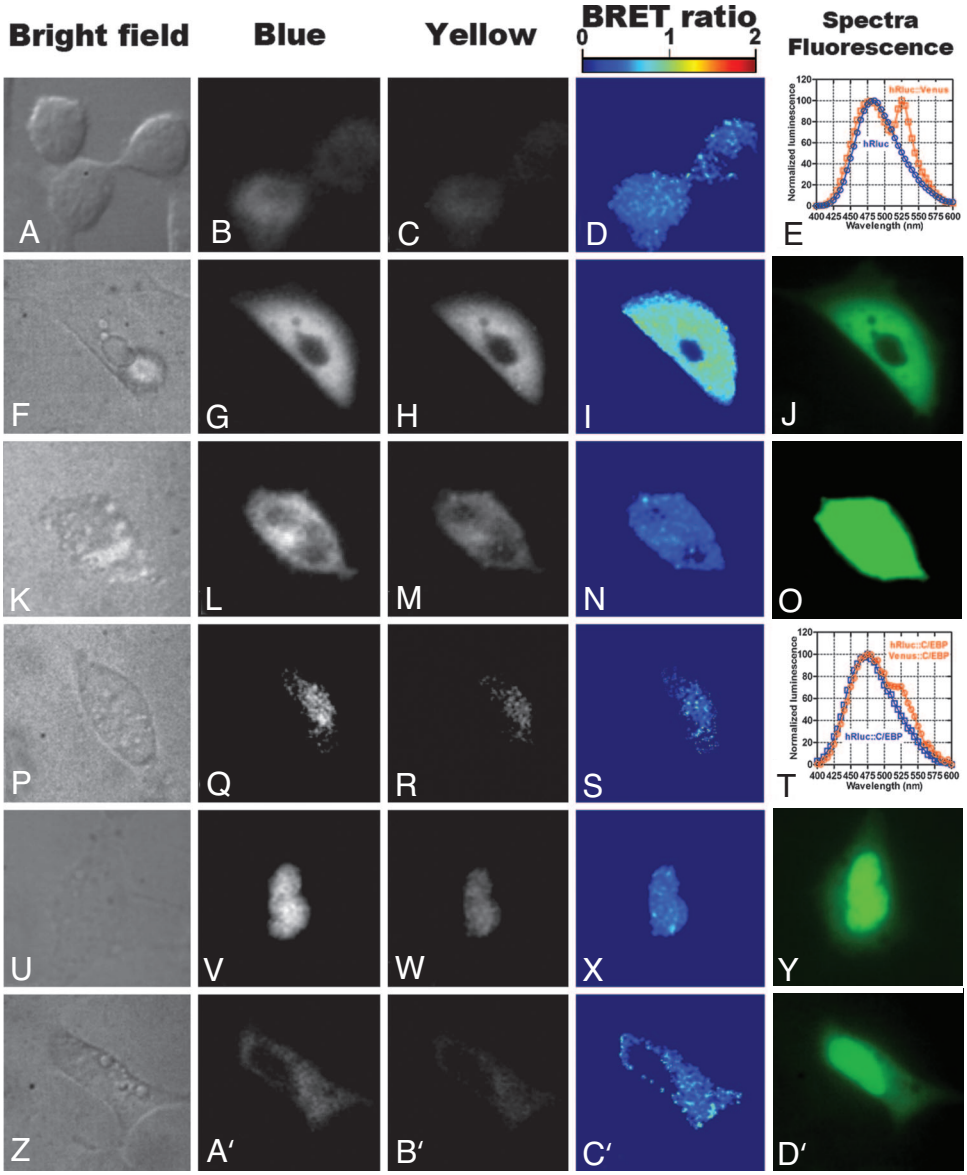

Fig. 4. Subcellular imaging of BRET in single mammalian cells. Cells were imaged with an Olympus IX71 microscope by using optics arrangement 3 with a ×60 oil immersion objective (NA 1.45). The luminescence images are integrations of 20 sequential 100-msec exposures. Cells were treated with 10 μM ViviRen in DMEM with 10% FBS (36°C). (*A–D*) HEK293 cells expressing hRLUC; Y÷B = 0.32 ± 0.05 SD (n = 10) over the luminescent portion of the cell. (*E*) Spectra of hRLUC versus hRLUC·Venus emission from HEK293 cells. (*F–J*) HEK293 cells expressing hRLUC·Venus; Y÷B = 0.82 ± 0.07 SD (n = 8) over the luminescent portion of the cell. (*K–O*) HEK293 cells expressing unfused hRLUC and Venus; Y÷B = 0.36 over the luminescent portion of this cell. (*P–S*) Mouse GHFT1 cells expressing hRLUC·C/EBPα; Y÷B = 0.24 ± 0.06 SD (n = 11) over the luminescent portion of the cell. (*T*) Spectra of hRLUC·C/EBPα versus hRLUC·C/EBPα + Venus·C/EBPα emission from mouse GHFT1 cells. (*U–Y*) Mouse GHFT1 cells expressing hRLUC·C/EBPα + Venus·C/EBPα; Y÷B = 0.39 ± 0.04 SD (n = 9) over the luminescent portion of the cell. (*Z–D′*) Mouse GHFT1 cells expressing hRLUC + Venus·C/EBPα; Y÷B = 0.30 over the luminescent portion of this cell. *A*, *F*, *K*, *P*, *U*, and *Z* are bright-field images; *B*, *G*, *L*, *Q*, *V*, and *A′* are blue luminescence images; *C*, *H*, *M*, *R*, *W*, and *B′* are yellow luminescence images; *D*, *I*, *N*, *S*, *X*, and *C′* are BRET ratios (Y÷B) over the entire image (pseudocolor scale shown above *D*); and *J*, *O*, *Y*, and *D′* are fluorescence images from Venus in fusion proteins.

SD) over the image (Fig. 4*D*). On the other hand, HEK293 cells transfected with the fusion protein hRLUC·Venus (Fig. 4 *F–J*) show a strong BRET ratio of 0.82 (Y:B = 0.82 ± 0.07 SD; Fig. 4*I*). To determine whether the BRET ratio is perturbed by expression of noninteracting proteins, we coexpressed unfused hRLUC and unfused Venus and found a low BRET ratio that indicates no spurious interaction (Y:B = 0.36; Fig. 4 *K–O*).

Furthermore, we have been able to image the subcellular distributions of interactions of the C/EBPα in single isolated mammalian cells. C/EBPα is a transcriptional factor that localizes to the heterochromatin in the nucleus and dimerizes (12, 13). A C/EBPα·hRLUC fusion protein localizes to the nucleus of mouse GHFT1 cells and demonstrates a low BRET ratio (Y:B = 0.24 ± 0.05 SD; Fig. 4 *P–S*). When C/EBPα·hRLUC is coexpressed with C/EBPα·Venus, however, the nuclear expression consistently reveals a higher BRET ratio within the nucleus (Y:B = 0.39 ± 0.04 SD; Fig. 4 *U–Y*). These observations confirm FRET studies of C/EBPα dimerization in GHFT1 cells that display nuclear regions of increased C/EBPα interaction (12). It is interesting to note that the fusion of C/EBPα to RLUC appears to influence the spectrum of RLUC emission slightly, as demonstrated by the reduction of the BRET ratio as compared with the RLUC control (Y:B = 0.24 versus 0.32). This observation illustrates

the importance of using the appropriate control for BRET studies. Coexpression of unfused hRLUC with Venus·C/EBPα is another control to demonstrate the absence of spurious interaction; as shown in Fig. 4*C′*, the BRET ratio of hRLUC essentially is the same (Y:B = 0.30) in the cytoplasm as the hRLUC control in Fig. 4*D* (Y:B = 0.32) despite the expression of Venus·C/EBPα that is localized prominently to the nucleus but is also found in the cytoplasm (Fig. 4*D′*). Another interesting observation is that hRLUC or hRLUC·Venus sometimes appears to be excluded from the nucleus in mammalian cells (e.g., Fig. 4 *G–J* and *A′–C′*), whereas it entered the *Arabidopsis* nucleus (the bulge at the 10 o'clock position of the ring; Fig. 2 *J–N*). However, when hRLUC or Venus is fused to C/EBPα, it is able to translocate to the mammalian nucleus (Fig. 4 *Q–S*, *V–Y*, and *D′*). Finally, the BRET ratio is independent of the brightness of the luminescence signal; thus, the BRET ratio is not influenced by the level of expression of donor (RLUC) or acceptor (e.g., Venus or YFP; see *SI Text* and SI Fig. 7).

Discussion

Fluorescence techniques have become the predominant methodology for imaging cells, subcellular organelles, and small pieces of tissue. This technology has blossomed, leading to fluorescence tools such as FRET, fluorescence photobleaching, fluorescence lifetime imaging, confocal microscopy, etc. (3). On the other hand, because of its exquisite sensitivity and independence from excitation, luminescence technology often is preferable for high-throughput screening (7). An additional advantage of BRET is that it is superior for deep penetration of animal tissues (6). Luminescence is also favored over fluorescence for assays of promoter activity, especially for those involving temporal changes of promoter activity, because native luciferases tend to have a shorter half-life than native fluorescent proteins do and therefore are better reporters of time-dependent changes (14) [there are destabilized fluorescent proteins that have shorter half-lives, but they still are not as useful for time-course experiments in which cells are irradiated frequently, leading to phototoxicity (15)].

Therefore, BRET outshines FRET in applications where fluorescence excitation is undesirable. The major limitation that has caused luminescence imaging to lag behind fluorescence imaging has been the fact that luminescence signals usually are much dimmer than fluorescence signals are. However, our application of a modified EB-CCD camera coupled with a microimager demonstrates that BRET now can be imaged at tissue, cellular, and even subcellular levels. At the subcellular level, we show that nuclear and cytoplasmic BRET signals can be visualized (Figs. 2 and 4). With this technology, it should be possible to visualize mitochondrial and chloroplastidic BRET signals as well. We have applied this technology to image protein interaction of (*i*) COP1 in plant seedlings, and (*ii*) C/EBPα in the mammalian nucleus. We also show that tissues that absorb light differentially can be used for quantitative measurements of BRET by a correction using RLUC·EYFP emission profiles. Together with the demonstration that BRET imaging is possible in tissues of intact animals (6), our results enable a host of applications for imaging without fluorescent excitation, thereby avoiding the problems of photobleaching, autofluorescence, phototoxicity, and undesirable stimulation of photobiological processes.

Materials and Methods

Plant and Mammalian Cell Culture. *Arabidopsis* and tobacco plant seedlings were transformed with expression cassettes of P_{35S}::RLuc, P_{35S}::RLuc·EYFP, and P_{35S}::RLuc·COP1 + P_{35S}::EYFP·COP1 (10). Plant seedlings were grown on 1/2 MS medium for 5–7 days (after germination) separately before measuring luminescence spectra and imaging. Single cells of *Arabidopsis* were generated from cell suspensions initiated from calli. Human HEK293 and mouse GHFT1 cells were grown in DMEM with 10% FBS at 37°C and transfected with plasmids using Lipofectamine 2000 (Invitrogen, Carlsbad, CA). After 24 h, cells were washed and resuspended in DMEM with 10% FBS for imaging. Plasmids were insertions into pcDNA3.1 with the transgenes expressed under the control of the CMV promoter P_{CMV}. See *SI Text* for details.

BRET Methods. Methods for measuring protein interactions in populations of cells with BRET have been described for bacteria (4, 16), plants (10, 17), and mammalian cells (6, 18–20). In this study, substrates for RLUC were native coelenterazine (NanoLight, Pinetop, AZ), ViviRen/EnduRen (Promega, Madison, WI), or Deep Blue C (BioSignal; PerkinElmer, Waltham, MA). For spectral measurements of BRET emission, a QuantaMaster QM-7/SE (Photon Technology International, Birmingham, NJ) spectrophotometer was used; for luminescence spectral measurements, the excitation beam was blocked, and the slit width was set to 16 nm.

Imaging of BRET. BRET imaging was accomplished by using (*i*) a Dual-View microimager, and (*ii*) a modified EB-CCD camera. The Dual-View microimager (Optical Insights, Tucson, AZ) allows the simultaneous acquisition of luminescence images at two wavelengths. It consists of a dichroic mirror (in our case, to split at 505 nm with Q505LPxr) and interference filters to select for wavelengths <505 nm (HQ505SP; blue) and for wavelengths >505 nm (HQ505LP; yellow). Our EB-CCD camera had a GaAsP photocathode with low-ion feedback and cooling to −25°C (Hamamatsu Photonic Systems, Bridgewater, NJ) (see *SI Text* for details). The acquisition software was Photonics-WASABI (Hamamatsu). BRET imaging of plant seedlings was performed both in a light-tight box and through an inverted microscope. In the case of the light-tight box setup (used for Figs. 1 and 3), the EB-CCD camera was coupled to the Dual-View to which a ×4 noninfinity-corrected microscopic objective had been attached, and the entire apparatus was enclosed in the light-tight box. This apparatus did not allow excitation of fluorescence. For plant seedlings, cells, and mammalian cells, the Dual-View and EB-CCD were attached to the bottom port of an IX-71 inverted microscope (Olympus America Inc., Melville, NY). This setup allows the measurement of fluorescence with an epifluorescence attachment (excitation 500/20 nm, emission 520 long pass). The entire IX-71 microscope was enclosed in a temperature-controlled (22–37°C) light-tight box. For low-power imaging (e.g., Fig. 2 *B–I*), a Macro XLFLuor ×2 objective, numerical aperture (N.A.) 0.14 (Olympus) was used (optics arrangement 1), whereas for higher magnifications, a UPlanFl ×40 objective, N.A. 1.30 (oil immersion, Olympus) was used for Fig. 2 *J–N* (optics arrangement 2), or a Plan Apo ×60 objective, N.A. 1.45 (oil immersion, Olympus) was used for Fig. 4 (optics arrangement 3). For luminescence imaging of plant seedlings and cells, a single exposure (5–7.5 min) was taken; for single mammalian cells, 20 sequential 100-msec exposures were integrated by choosing the median value for each pixel over the sequence of 20 exposures. These integrations and the BRET ratio (Y:B) was calculated by using ImageJ. See *SI Text* for details.

We thank Dr. R. N. Day (University of Virginia, Charlottesville, VA) for mouse GHFT1 cells and C/EBPα 244 fused to EYFP; Dr. Roger Tsien (University of California at San Diego, La Jolla, CA) for Venus YFP; Drs. Michael Geusz, David Piston, Yao Xu, and Shin Yamazaki for advice concerning imaging and image analysis; and Drs. Keith Wood and Erika Hawkins (Promega, Madison, WI) for making ViviRen available to us before its commercial release. This work was supported by National Science Foundation Grant MCB-0114653 (to A.G.v.A. and C.H.J.) as part of the *Arabidopsis* 2010 project and by National Institutes of General Medical Science Grant R01 GM065467 (to C.H.J.).

1. Mendelsohn AR, Brent R (1999) *Science* 284:1948–1950.
2. Förster T (1948) *Annalen Der Physik* 2:55–75.
3. Periasamy A, Day RN (2005) *Molecular Imaging: FRET Microscopy and Spectroscopy*, eds Periasamy A, Day RN (Oxford Univ Press, New York), p 321.
4. Xu Y, Piston DW, Johnson CH (1999) *Proc Natl Acad Sci USA* 96:151–156.
5. Morin JG, Hastings JW (1971) *J Cell Physiol* 77:313–318.
6. De A, Gambhir SS (2005) *FASEB J* 19:2017–2019.
7. Milligan G (2004) *Eur J Pharm Sci* 21:397–405.
8. Dixit R, Cyr R, Gilroy S (2006) *Plant J* 45:599–615.
9. Pfleger KD, Eidne KA (2006) *Nat Methods* 3:165–174.
10. Subramanian C, Kim BH, Lyssenko NN, Xu X, Johnson CH, von Arnim AG (2004) *Proc Natl Acad Sci USA* 101:6798–6802.
11. von Arnim AG, Osterlund MT, Kwok SF, Deng XW (1997) *Plant Physiol* 114:779–788.
12. Day RN, Periasamy A, Schaufele F (2001) *Methods* 25:4–18.
13. Demarco IA, Periasamy A, Booker CF, Day RN (2006) *Nat Methods* 3:519–524.
14. Hastings JW, Johnson CH (2003) in *Biophotonics*, *Part A*, *Methods in Enzymology*, eds Mariott AG, Parker I (Elsevier Academic, San Diego), pp 75–104.
15. Nagoshi E, Saini C, Bauer C, Laroche T, Naef F, Schibler U (2004) *Cell* 119:693–705.
16. Xu Y, Piston D, Johnson CH (2002) in *Green Fluorescent Protein: Applications and Protocols* (*Methods in Molecular Biology Series*), ed Hicks BW (Humana Press, Totowa, NJ), pp 121–133.
17. Subramanian C, Woo J, Cai X, Xu X, Servick S, Johnson CH, Nebenführ A, von Arnim AG (2006) *Plant J* 48:138–152.
18. Angers S, Salahpour A, Joly E, Hilairet S, Chelsky D, Dennis M, Bouvier M (2000) *Proc Natl Acad Sci USA* 97:3684–3689.
19. Gales C, Rebois RV, Hogue M, Trieu P, Breit A, Hebert TE, Bouvier M (2005) *Nat Methods* 2:177–184.
20. Soutto M, Xu Y, Johnson CH (2005) in *Molecular Imaging: FRET Microscopy and Spectroscopy*, eds Periasamy A, Day RN (Oxford Univ Press, New York), pp 260–271.

Supporting Information

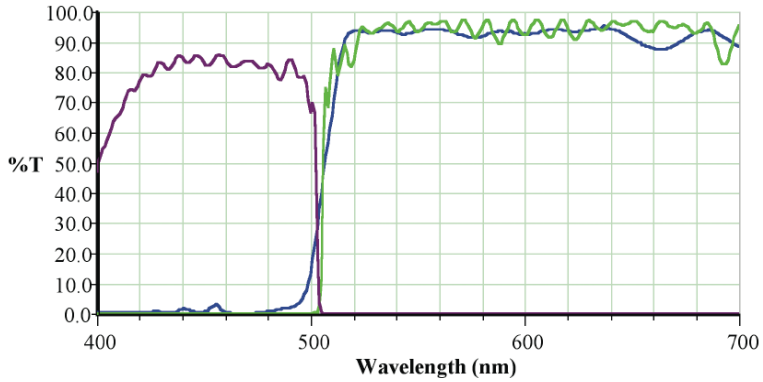

Fig. 5. Spectra of the filters and dichroic in our Dual-View image splitter. Traces are as follows: blue curve, Q505LPxr (lot 23491) = dichroic mirror; green curve, HQ505LP (lot 36429) = long-pass filter for yellow (Y); and purple curve, HQ505SP (lot 43815) = short-pass filter for blue (B).

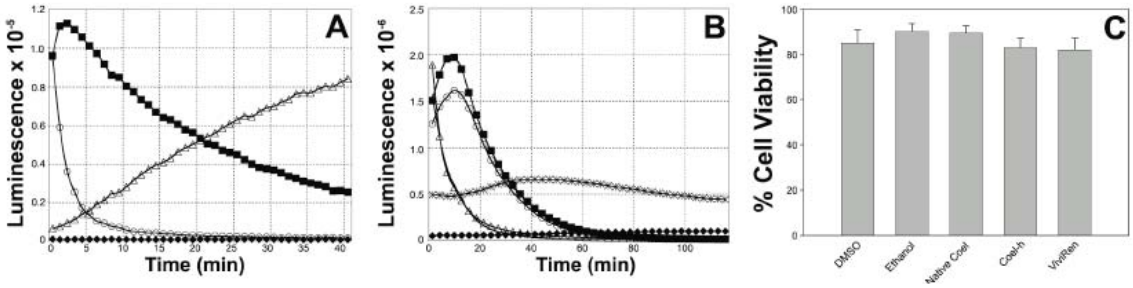

Fig. 6. Comparison of coelenterazine substrates. (*A*) Autoluminescence of substrates in DMEM with and without 10% FBS (no cells present): for 10 mM native coelenterazine, filled squares = DMEM + 10% FBS and open circles = DMEM without FBS; for 10 mM ViviRen, open triangles = DMEM + 10% FBS and filled diamonds = DMEM without FBS. (*B*) Brightness of enzyme-catalyzed luminescence with native vs. ViviRen coelenterazine. For HEK293 cells in DMEM + 10% FBS and transfected with P_{CMV}::hRluc•Venus: line without symbols = 5 mM native coelenterazine, open triangles = 10 mM native coelenterazine, open circles = 5 mM ViviRen, filled squares = 10 mM ViviRen. For tobacco seedlings transfected with P_{35S}::Rluc•EYFP in 1/2 MS medium: x = 10 mM native coelenterazine, filled diamonds = 10 mM ViviRen. Note the ordinal scale difference between *A* and *B*. (*C*) HEK293 cell viability after exposure to three different substrates. Cell viability was assayed by trypan blue exclusion after exposure to substrates and/or solvents for 1 h (6 h data essentially is the same). HEK293 cells were in DMEM + 10% FBS. Data are shown as % viability (±SEM) as compared with untreated cells. Treatments were: 0.1% DMSO, 0.1% ethanol, 10 mM native coelenterazine (0.1% ethanol final concentration), 10 mM coelenterazine-h (0.1% ethanol final concentration), and 10 mM ViviRen (0.1% DMSO final concentration).

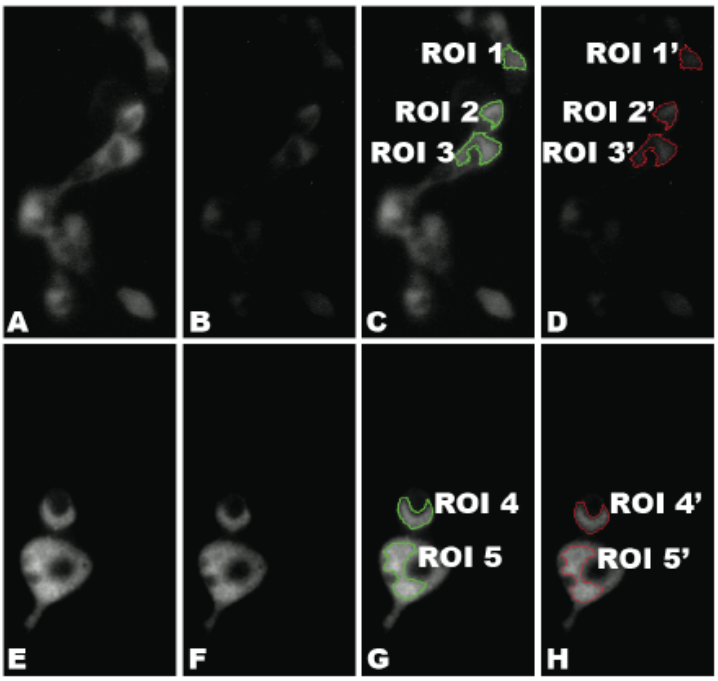

Fig. 7. BRET ratio is not affected by the intensity of luminescence of hRLUC (*A*--*D*) or hRLUC•Venus (*E*--*H*) in HEK293 cells. *A* and *E* are the luminescence at 480 nm (B); *B* and *F* are the luminescence at 530 nm (Y); *C* and *D* show the cell Regions of Interest (ROIs) calculated from *A* and *B*, respectively; and *G* and *H* show the cell ROIs calculated for *E* and *F*, respectively. The BRET ratios for each of these cell ROIs are: ROI 1 = 0.34, ROI 2 = 0.33, ROI 3 = 0.34, ROI 4 = 0.81, and ROI 5 = 0.79.

SI Text

Plant Transformation and Cell Line Generation. *Arabidopsis* (*Arabidopsis thaliana*) and tobacco (*Nicotiana tabacum* cv. Xanthi) were transformed with T-DNA expression cassettes of 35S::RLuc (pBIN19 Rluc), 35S::RLuc•EYFP(pBIN19 Rluc:EYFP), and 35S::RLuc•COP1(N) + 35S::EYFP•COP1(N){pPZP222 Rluc•Cop1(N) ´ pBin19 EYFP•Cop1(N); "N" being N terminus; te COP1 constructs lacked the C-terminal WD40 domain} (1) by Agrobacterium-mediated transformation (*Agrobacterium tumefaciens* strain GV3101) (2, 3). The tobacco cotransformation lines with two independent T-DNAs RLuc-COP1(N)/EYFP-COP1(N) were screened on gentamycin and kanamycin media. Both tobacco and *Arabidopsis* seedlings were grown on 1/2 MS medium for 7 and 5 days (after germination) separately before measuring luminescence spectra and imaging. *Arabidopsis* calli were induced by germinating seeds directly on the induction medium containing 0.5 mg/liter 2,4-D(2,4-dichloro-phenoxyacetic acid), 2.0 mg/liter a-naphthaleneacetic acid (NAA), 0.5 mg/liter 6-BA(6-benzylamino-purine) (Sigma). Cell suspension lines were initiated by transferring the callus to 20 ml of fresh induction medium in a flask and placing it on a shaker (120 rpm, 22°C, 12-h light/12-h dark cycle) (4). Single cells of *Arabidopsis* were generated from these cell suspensions initiated from calli. BRET constructs were expressed under the control of the constitutive promoter CaMV 35S (P_{35S}).

Mammalian Cell Culture and Transfection. Human HEK293 and mouse GHFT1 cells were grown in DMEM (Sigma) with 10% FBS at 37°C and transfected with plasmids using Lipofectamine 2000 (Invitrogen) as follows. Four micrograms of plasmids were mixed with 10 ml of Lipofectamine 2000 in 250 ml of OptiMEM medium. This mixture was added to cells in a 35-mm dish containing 2 ml of DMEM + 10% FBS. After 24-48 h, cells were washed and resuspended in DMEM with 10% FBS for imaging.

Plasmids were insertions into pcDNA3.1 with the transgenes expressed under the control of the CMV promoter P_{CMV}. Venus YFP and C/EBPa244 were amplified from their original vectors by PCR. PCR primers were designed to create specific restriction enzyme sites in each PCR product. These fragments were purified and subcloned in the corresponding restriction sites into hRlucC1 (codon "humanized" pRlucC1 from Perkin-Elmer) or the pcDNA 3.1+ vector (Invitrogen) to create different plasmids that express hRluc•Venus, hRluc•C/EBPa244, and Venus•C/EBPa244 fusion proteins under the control of the CMV promoter P_{CMV}.

Spectral Measurements. For spectral measurements of BRET emission, a QuantaMaster QM-7/SE (Photon Technology International, Birmingham NJ) spectrophotometer was used; for luminescence spectral measurements, the excitation beam was blocked and the slit width was set to 16 nm.

Imaging of BRET. Methods for measuring protein interactions in populations of cells using BRET have been described for bacteria (5, 6), plants (1, 7), and mammalian cells (8-11). Our imaging setup consisted of a Dual-View, an EB-CCD camera, and, in all figures except Fig. 1, an inverted microscope. These components and arrangements are described below.

Dual-View microimager: The Dual-View microimager (Optical Insights, Tucson AZ) allows us to collect images in two wavelength ranges simultaneously; therefore, a BRET ratio of emission in the two ranges can be calculated without the complication that the total luminescence signal may be changing over the time course of the exposure. The Dual-View includes a dichroic mirror that splits the image at 505 nm and short-pass/long-pass filters that refine the spectral distinction. The part numbers of the dichroic mirror and interference filters we used are as follows:

Filters: HQ505SP and HQ505LP

Dichroic mirror: Q505LPxr

Camera: We used a modified electron bombardment-charge-coupled device (EB-CCD) camera (Hamamatsu Photonic Systems, Bridgewater NJ); the modifications were a GaAsP photocathode with low ion feedback and increased photocathode cooling to

-25°C. The low ion feedback was achieved by a special modification to the EB-CCD camera by Hamamatsu to remove the aluminum mask from the sensor that normally is included to avoid the "double-focus phenomenon." In the case of low-light imaging, this problem is negligible. In addition, the camera is using full-frame transfer CCD, so it is possible to remove the mask. As a result, the sensor gets the same gain at a lower acceleration voltage. This low acceleration voltage reduces the ion feedback phenomenon drastically, improving performance for very low-light level imaging. Finally, the cooling of the photocathode to -25°C reduces the dark current of the photocathode. The acquisition software was Photonics-WASABI (Hamamatsu).

"Box" setup: In this arrangement, samples were enclosed in a light-tight box. The EB-CCD camera was coupled to the Dual-View image splitter, which was coupled directly to a non-infinity-corrected microscopic objective (Plan 4´, NA = 0.13 DL, 160/- or Plan 10´, NA = 0.30 DL, 160/0.17; Nikon). Fluorescence imaging was not possible when using this setup. Under these conditions, spontaneous YFP fluorescence or autofluorescence in the absence of coelenterazine (as might occur if there were a light leak) could not be detected in the light-tight box setup for 10- to 30-min exposures. After adding coelenterazine to the seedlings, images then were detectable by the EB-CCD camera for exposures of 5 min or less.

Microscope setup: In this arrangement, samples were viewed through an IX-71 inverted microscope (Olympus America Inc., Melville NY) with epifluorescence attachment, excitation (EX) 500/20 nm, emission (EM) 520 LP. The EB-CCD camera was coupled to the Dual-View image splitter, which was connected to the bottom port of the IX-71 microscope. The microscope (but not the EB-CCD camera or Dual-View) was placed in a light-tight, temperature-controlled box (the same controls in the absence of

coelenterazine were performed for the microscope setup as mentioned above for the box setup with the same results). The entire microscope/apparatus was maintained at 22°C for plant tissue and at 36°C for mammalian cell imaging.

Optics arrangement 1: Macro XLFLuor 2´ objective, NA 0.14 (Olympus)

Optics arrangement 2: UPlanFl 40´ objective, NA 1.30 (oil immersion, Olympus)

Optics arrangement 3: Plan Apo 60´ objective, NA 1.45 (oil immersion, Olympus # 1-U2B616)

For BRET imaging of plants, seedlings were soaked in 10 mM native coelenterazine for immediate measurement. *Arabidopsis* cotyledons and single cells were imaged with optics arrangements 1 or 2 through the inverted microscope (IX71, Olympus). Mammalian cells were imaged with optics arrangement 3. The microscope was equipped with a UV light source (BH2-RFL-T3, Olympus) and an EX-HQ 500/20 fluorescent filter (EM 515 nm, Olympus) to acquire the fluorescence of YFP-expressing seedlings and cells. Tobacco seedlings were imaged through 4´ and 10´ non-infinity-corrected objectives attached directly to the Dual-View in the Box setup. BRET signals were collected with the cooled (-25°C) EB-CCD camera and the Dual-View (Optical Insights, LLC) combination imaging system.

The BRET images of blue light (<505 nm = B) and yellow light (>505 nm = Y) were acquired simultaneously through the Dual-View (dichroic = Q505LPxr, interference filters HQ505SP and HQ505LP, exposure time 5-10 min). The images acquired by the camera were 16-bit TIF files. For mammalian cells, 20 sequential 100-ms exposures were placed into a stack in ImageJ (version WCIF) and integrated by choosing the median value for each pixel over the sequence of 20 exposures. For luminescence imaging of plant seedlings and cells, a single exposure (5-7.5 min) was taken (because the imaging of plant seedlings and cells was at the limit of detection of the luminescence signal, integration of multiple exposures was not performed on the plant samples). Then for both plant and mammalian samples, background subtraction was performed with ImageJ by using a single pixel from the nonsample region of the image as a background value. As part of the background subtraction, the files are converted to 8-bit TIF format. Then, the Y and B images were aligned with ImageJ and a pixel-by-pixel ratio (Y¸B) was calculated with ImageJ. These numerical ratios were visualized with a pseudocolor look-up table (LUT) as displayed on our figures.

Correction of BRET emission for tissue absorption of light (tobacco): In Fig. 3*C*, the absorption of an ethanol extract of total pigments from tobacco seedlings [both pigmented from light-grown (green) and essentially unpigmented from dark-grown (etiolated) seedlings] was measured. The absorption ratio 480:530 was 2.07 for green seedlings and 1.63 for etiolated seedlings. Therefore, to provide a correction factor:

2.07 ¸ 1.63 = 1.27.

This correction factor correlates well with the inhibition of the 480-nm emission by the green tissue seen in Fig. 3*B* (when the 530-nm peak is normalized to 1.0 and assuming that the 480- and 530-nm peaks should be roughly equal), which is 1.31.

Comparison of Native Coelenterazine, Deep Blue C, and ViviRen for BRET Imaging. In the experiments with plants depicted in Figs. 1-3, we used native coelenterazine as the substrate for RLUC. Native coelenterazine is nontoxic and highly permeable to all cell types that we have tested (we obtained native coelenterazine from Nanolight). Recently, new analogs of coelenterazine have become available commercially that potentially are useful for BRET. Two of these, EnduRen (Promega) and Deep Blue C (BioSignal/PE), generate luminescence that was too dim to be useful for imaging under our conditions. On the other hand, ViviRen (Promega) has been useful for BRET imaging of single mammalian cells, as in Fig. 4. ViviRen is a modified version of the coelenterazine analog, coelenterazine-h, to which ester groups have been added. The original design intention of ViviRen was to develop an inactive RLUC substrate that would not undergo autoluminescence due to oxidation (a significant problem for native coelenterazine in

serum-containing medium, Fig. 6*A*) but that would permeate into cells where intracellular esterases cleave the ester groups to generate active coelenterazine-h. In our tests, we find that ViviRen has slightly less autoluminescence than native coelenterazine in serum-containing medium for the first 15-20 min but that its autoluminescence level steadily increases so that after 20 min, it has more autoluminescence than native coelenterazine (Fig. 6*A*). In serum-free medium, native coelenterazine has a brief burst of autoluminescence upon addition, but thereafter both native and ViviRen coelenterazine have low autoluminescence (Fig. 6*A*). HEK293 cells transfected with BRET constructs have brighter luminescence when using ViviRen than when using native coelenterazine in serum-containing medium during the interval 5-50 min after addition (Fig. 6*B*). At 10 min after addition, the signal from cells expressing hRLUC•Venus is 100´ higher than the autoluminescence when using ViviRen. The viability of cells was not significantly affected by treatment for 1-6 h with either native coelenterazine or ViviRen (Fig. 6*C*). Therefore, for HEK293 cells in 10% FBS (*i*) signal:autoluminescence and (*ii*) signal stability were superior with ViviRen as compared with native coelenterazine, and it therefore was used in the imaging experiments depicted in Fig. 4. On the other hand, ViviRen does not appear to be useful for BRET in plant seedlings. The autoluminescence of native and ViviRen coelenterazines in the simple salt medium (1/2 MS) was comparable to that of serum-free DMEM (Fig. 6*A*), but ViviRen did not enhance the signal from tobacco seedlings expressing BRET constructs (Fig. 6*B*). Native coelenterazine in1/2 MS medium allows a long-term, stable BRET signal from tobacco seedlings (Fig. 6*B*).

Assay for the effect of substrates on mammalian cell viability: HEK293 cells were grown in 24-well plates to the same density overnight. The next day, the cells were washed, and the medium was changed to medium with or without serum. At this time the cells were 80% confluent. The cells were incubated for 1 h with different substrates: native coelenterazine, coelenterazine-h, and ViviRen. Coelenterazine and coelenterazine-h were dissolved in ethanol, and ViviRen was dissolved in DMSO. Final concentrations were 5 mM for coelenterazine and coelenterazine-h and 10 mM for ViviRen. After the incubation, the cells were harvested, and 0.1 ml of 0.4% (wt/vol) trypan blue was added to 0.1 ml of the cell suspension from each sample. The stained and unstained cells were counted by using a hemacytometer. Blue-stained cells were scored as nonviable, and unstained cells were scored as viable. Therefore, percentage viability = number of viable cells ¸ total number of cells.

BRET Ratio Is Independent of Luminescence Intensity. To demonstrate that the BRET ratio is not influenced by the level of total luminescence, we calculated the BRET ratio for cells of different total luminescence from the same image capture. Fig. 7 shows that (*i*) three HEK293 cells transfected with hRLUC and exhibiting different intensities of luminescence had BRET ratios (Y¸B) of 0.33-0.34 (compare with Fig. 4*D*, where Y¸B = 0.32 ± 0.05 SD) and (*ii*) two HEK293 cells transfected with hRLUC•Venus and exhibiting different intensities of luminescence had BRET ratios (Y¸B) of 0.81 and 0.79 (compare with Fig. 4*I*, where Y¸B = 0.82 ± 0.07 SD). We conclude that BRET ratios are consistent for cells transfected with the same constructs and for cells exhibiting different levels of expression of those constructs.

1. Subramanian C, Kim BH, Lyssenko NN, Xu X, Johnson CH, von Arnim AG (2004) *Proc Natl Acad Sci USA* 101:6798-6802.

2. Clough SJ, Bent AF (1998) *Plant J* 16:735-743.

3. An G, Watson BD, Chiang CC (1986) *Plant Physiol* 81:301-305.

4. Mathur J, Koncz C (1998) in *Arabidopsis Protocols*, eds Martinez-Zapater JM, Salinas J (Humana Press, Totowa, NJ), pp 27-30.

5. Xu Y, Piston DW, Johnson CH (1999) *Proc Natl Acad Sci USA* 96:151-156.

6. Xu Y, Piston D, Johnson CH (2002) in *Green Fluorescent Protein: Applications and Protocols (Methods in Molecular Biology Series*), eds Hicks BW (Humana Press, Totowa, NJ), pp 121-133.

7. Subramanian C, Woo J, Cai X, Xu X, Servick S, Johnson CH, Nebenführ A, von Arnim AG (2006) *Plant J* 48:138-152.

8. Angers S, Salahpour A, Joly E, Hilairet S, Chelsky D, Dennis M, Bouvier M (2000) *Proc Natl Acad Sci USA* 97:3684-3689.

9. Gales C, Rebois RV, Hogue M, Trieu P, Breit A, Hebert TE, Bouvier M (2005) *Nat Methods* 2:177-184.

10. Soutto M, Xu Y, Johnson CH (2005) in *Molecular Imaging: FRET Microscopy and Spectroscopy*, eds Periasamy A, Day RN (Oxford Univ Press, New York), pp 260-271.

11. De A, Gambhir SS (2005) *FASEB J* 19:2017-2019.